Available online at www.sciencedirect.com
ScienceDirect
Mathematics and Computers in Simulation 167 (2020) 461–477
MATHEMATICS AND COMPUTERS IN SIMULATION
www.elsevier.com/locate/matcom

Original articles

An easy to implement and robust design control method dedicated to multi-cell converters using inter cell transformers

K. Tamizi, O. Béthoux*, E. Labouré

GeePs, Group of Electrical Engineering, Paris, France
UMR CNRS 8507, CentraleSupélec, Univ Paris-Sud, Sorbonne Universités, UPMC Univ Paris, 06 Gif-sur-Yvette, France

Received 15 January 2018; received in revised form 2 October 2018; accepted 1 February 2019
Available online 12 March 2019

Abstract

Parallel multi-cell converters using inter-cell transformers are real multi-input multi-output systems, making their control challenging and possibly requiring increased embedded computing power in the control architecture. The challenge of the current study is to design a control algorithm as simple as possible, in terms of settings and implementation, while meeting standard specification. The state-space representation of multi-cell converters permits to define a full state feedback. Such Multi-Input Multi-Output (MIMO) systems have numerous tuning parameters which enable various ways to tackle the control specifications. Among the specific approaches, both total decoupling and optimal control based on quadratic cost and objective functions are addressed thoroughly and consistently. The studied case is a 3-cell parallel converter for which various settings of the state feedback are considered and analyzed by simulation Linear-quadratic regulator design reveals the best compromise between variables tracking precision and robustness towards system parameters and load variation. Furthermore it is easy to implement utilizing few non-zero setting coefficients. Specifically the feedback gain matrix associated to the integral terms is almost diagonal: this natural decoupling makes it extremely simple to efficiently implement an anti-windup algorithm. This is an important result since until now, the standard solution is mostly based on decoupling strategies. Among other drawbacks, this latter approach proves to be much more sensitive to parameter uncertainties.

Keywords: Multicell converter; InterCell Transformer (ICT); Multi input multi output system (MIMO); Robust control; Linear quadratic regulator (LQR)

1. Introduction

Parallel multi-cell converters using inter cell transformers (ICTs) are an attractive technique in the field of low and medium voltage and high current power converters. These very versatile structures can be used in many types of power conversion structures such as Boost or Buck DC-to-DC power converters as well as in DC-to-AC inverters or AC-to-DC synchronized rectifiers. They are broadly used in various applications and are particularly useful in renewable energy systems such as in photovoltaic inverters [3,8], storage management systems [22], fuel cell converters [9] as well as in electrical vehicle [6]. Notwithstanding this success, there is scope for further

* Correspondence to: UPMC Univ Paris, France.
E-mail address: olivier.bethoux@centralesupelec.fr (O. Béthoux).

https://doi.org/10.1016/j.matcom.2019.02.004

improvements, such as ICT design for fault-operation [17] and control enhancement [2,7]. The present article focuses on this latter point from a control engineering practice point of view.

On a very broad basis, fractioning power shows many advantages. When interleaved generated Pulse Width Modulation (PWM) patterns are used, it enables to significantly reduce the switching stress due to interconnections leakage energy leading to voltage overshoot and electromagnetic interferences and the harmonic spectrum. This also allows a significant decrease of input and output filters size. The best performances are obtained in multi-cell converters when the converter is designed with one or several magnetic ICTs instead of individual inductors [11]. With respect to this final point, the ICT has to figure an important coupling effect to achieve good performances (compactness, power efficiency, current constraints). From a control point of view this magnetic coupling makes the power stage switch from several single input single output (SISO) systems to a unique multi input multi output (MIMO) system. Despite this change, the challenge is to keep the dedicated control algorithm as simple as possible, in terms of settings and implementation. It aims at providing an efficient control, both robust regarding system uncertainties and easy to implement in a classic microcontroller.

The literature shows that the study of the ICT multicell converter control has already been undertaken. First, Bolloch et al. have elaborated a strategy permitting a relevant steady state behavior without deeply studying the dynamic behavior of the control scheme [2]. Then, Gautier et al. have proposed a strategy based on decoupling matrices which permits to control the natural modes of the converter with independent PI controllers [7]. This unique solution based on a practical approach leads to a single solution which has not really been considered in a broader context permitting to assess its performances regarding other solutions. On a more specific issue, sensitivity analysis regarding parameters uncertainties are not assessed. Amghar et al. have explored another possible control technique based on a combination of PI controller and Petri nets method [1]. It requires very high sampling rates to operate properly and, in the submitted work, the magnetic coupling effect has not yet been taken into account. Based on Finite-state machine, Petri nets number of states increase exponentially with the number of cells, making it demanding on computational resources.

Among the previous studies, classical PI controllers can be achieved with relatively small computational resources. The accurate adjustment of their settings, the impact of system parameters uncertainties, the functioning under saturation have not been yet addressed. The present investigation is carrying out a comprehensive study of state-feedback controller. It considers the different ways to tune its control settings with respect to system parameter sensitivity, decoupling behavior and the ease of implementation including control during saturation. For this purpose, the ICT converter is studied in the general framework of state representation. The present work exhibits the available degrees of freedom and argues on their best use. The control performance criteria are assessed regarding parameter uncertainties in order to address robustness key issue. Specific focus is also given to implementation issues. In addition, the theoretical study is supplemented with simulation results based on a 3-cell ICT converter.

The manuscript is organized as follows. After this short introduction, Section 2 presents the control model of a 3-cell interleaved multi-cell buck converter and details the specifications related to the PV application under study. The third section presents the state feedback controller and considers the various possibility of tuning its numerous parameters. The fourth section addresses the particular tuning choice which permits to cancel coupling effects between the cells. The fifth section considers another design method based on the optimization of a quadratic optimization function, named LQR approach [5]. The sixth part undertakes a comprehensive comparative study of both considered approaches; for this purposes numerous scenarios are simulated and analyzed. Finally, the paper ends with conclusions and future prospects.

2. Multi-cell interleaved buck converter and its control-oriented model

2.1. Multi-cell interleaved buck converter for solar application

Fig. 1 depicts the system under study. A photovoltaic array feeds a load which could be possibly a battery directly powering DC loads or a grid inverter [13]. As both PV maximum power point and the load voltage can vary greatly, it is mandatory to interface a converter between the load and the source: this is the multi-cell converter using a monolithic ICT formed by n windings wounded on the same magnetic circuit. For simplicity, it has three switching cells ($n = 3$) and a 3-phase-transformer acting as an output current filter. The input current is filtered by the input capacitor C_i. Each switching cell is driven by a PWM control signal characterized by a constant switching

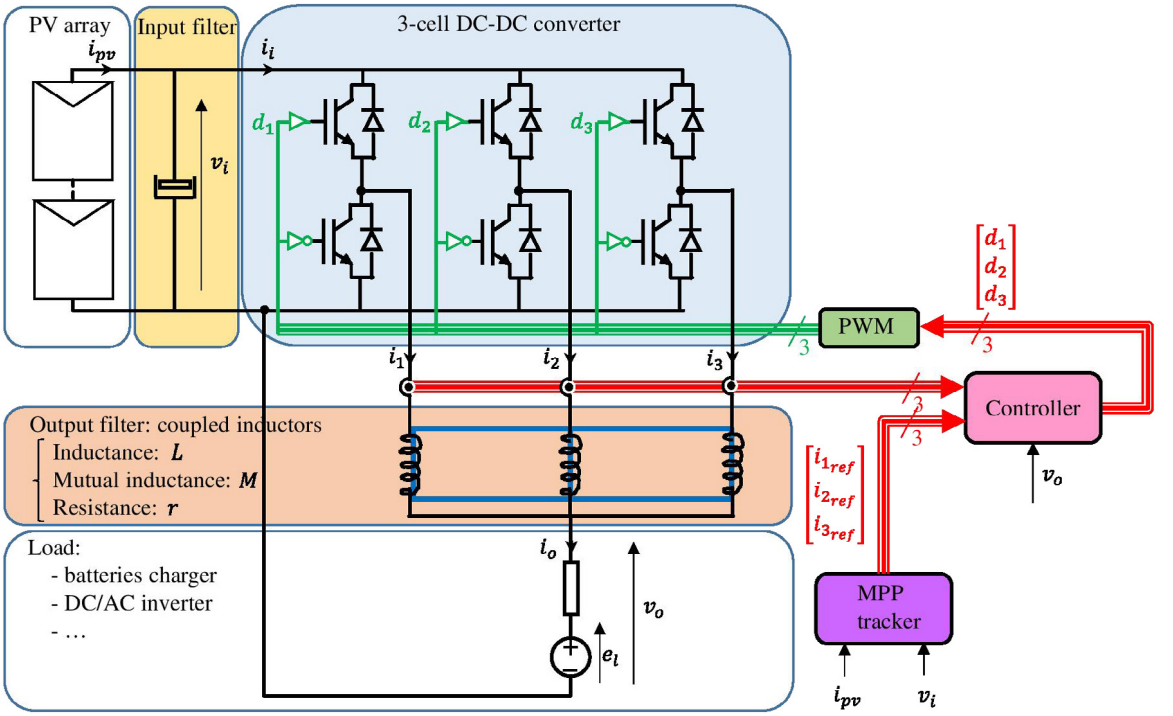

Fig. 1. Cell coupled power architecture.

frequency f and a duty cycle d_k, which represents a system control variable. The system parameters and the rated variables are listed in Table 1.

Compared to classic single buck converter, the main advantage of this power electronics structure is to ensure low current ripples at both input and output sides. In fact, regarding the input stage, the input current ripple is reduced by an n factor while the input current apparent frequency is increased by a factor of n. As a result, the C_i capacitance can be reduced by a significant n^2 factor leading to improve the system dynamics and namely its ability to track faster the maximum power point of the PV array. Similarly, the amplitude of phase current ripples are reduced by a n^2 factor compared to an uncoupled multi-cell converter (considering a similar filtering inductance value), which reduces the constraints on the power semi-conductors and the related losses. Moreover, the global power converter output current ripple is reduced by n compared to a classical one-cell Buck DC–DC converter, in the same way as for interleaved multi-cell DC–DC Buck converter with uncoupled inductors. This limits the need to filter the output voltage: in some cases, no additional output capacitor is required.

These electrical and energetics advantages are counterbalanced by a rising difficulty to control the system in static and dynamic conditions. This is why a control-orientated model is needed to study the feedback control.

2.2. Control-oriented models of multi-cell interleaved buck converter

For general purpose, the power converter model uses the following assumptions:

– Regarding the closed loop response time of the controlled system, PV array behaves as a perfect voltage source. The input voltage of the power converter v_i is therefore imposed in the model.
– The load fed by the power converter can represent different types of loads and is assumed to be linear. It is considered as a Thévenin's equivalent circuit consisting of an equivalent voltage source e_l in series connection with an equivalent impedance Z_l. The following developments only consider the pure real case, namely: $Z_l = r_l$. Finally, the DC load is hence described by:

$$v_o = e_l + r_l i_o \tag{1}$$

where v_o and i_o are the output voltage and current, respectively.

Table 1
System parameters.

Symbol	Quantity	Value
v_i	PV panel array voltage	400 (V)
$I_{i_{rated}}$	PV panel array current	9.25 (A)
f	Cell switching frequency	20 (kHz)
C_i	Input capacitance	2 (mF)
l	ICT self-inductance	20.0 (mH)
m	ICT mutual inductance	9.5 (mH)
r	ICT rated phase resistance	0.2 (Ω)
r_l	Rated load resistance	0 (Ω)
$i_{l,max}$	Short circuit current protect.	15 (A)
e_l	Rated load voltage source	200 (V)
l_{min}	Minimum ICT self-induct.	19.7 (mH)
m_{max}	Maximum ICT mutual induct.	9.7 (mH)
r_{max}	Maximum ICT phase resist.	0.5 (Ω)

– The monolithic ICT is also considered as linear and is represented by three magnetically coupled electrical equations. For a 3-leg symmetrical monolithic ICT the mutual inductances are identical with a negative value and are denoted $(-m)$ in the following model while l is the winding self-inductance:

$$\begin{bmatrix} v_{L1} \\ v_{L2} \\ v_{L3} \end{bmatrix} = \begin{bmatrix} l & -m & -m \\ -m & l & -m \\ -m & -m & l \end{bmatrix} \frac{d}{dt} \begin{bmatrix} i_1 \\ i_2 \\ i_3 \end{bmatrix} + \begin{bmatrix} r & 0 & 0 \\ 0 & r & 0 \\ 0 & 0 & r \end{bmatrix} \begin{bmatrix} i_1 \\ i_2 \\ i_3 \end{bmatrix} \tag{2}$$

– The 3 switching cells are controlled by 3 binary control variables u_k, operating at a constant switching frequency T_S. For the purpose of designing a control scheme, only the average cell behavior is considered; the system control inputs are the 3 duty-cycles of each cell $d_k = \langle u_k \rangle_{T_S}$ which have a limited range from 0 to 1. Duty cycles saturation should therefore be managed by the controller. This technical point has to be taken into account properly to obtain an efficient real-time implementation.

With these assumptions, the Kirchhoff's current law gives the link between output current and ICT's inner currents:

$$i_o = i_1 + i_2 + i_3 \tag{3}$$

while the 3 Kirchhoff's voltage laws of the global system show the link between control values d_k, output voltage v_o and inner ICT's voltages v_{Lk}:

$$v_i \begin{bmatrix} d_1 \\ d_2 \\ d_3 \end{bmatrix} = \begin{bmatrix} v_{L1} \\ v_{L2} \\ v_{L3} \end{bmatrix} + \begin{bmatrix} v_o \\ v_o \\ v_o \end{bmatrix} \tag{4}$$

Using previous equations, namely (1) to (4) enables to obtain the converter average model. It is written in the state-space representation as follows:

$$\begin{aligned} \frac{d}{dt} \begin{bmatrix} i_1 \\ i_2 \\ i_3 \end{bmatrix} = & -\frac{1}{(l-2m)(l+m)} \begin{bmatrix} l-m & m & m \\ m & l-m & m \\ m & m & l-m \end{bmatrix} \begin{bmatrix} r+r_l & 0 & 0 \\ 0 & r+r_l & 0 \\ 0 & 0 & r+r_l \end{bmatrix} \begin{bmatrix} i_1 \\ i_2 \\ i_3 \end{bmatrix} \\ & + \frac{v_i}{(l-2m)(l+m)} \begin{bmatrix} l-m & m & m \\ m & l-m & m \\ m & m & l-m \end{bmatrix} \begin{bmatrix} d_1 \\ d_2 \\ d_3 \end{bmatrix} - \frac{1}{(l-2m)} \begin{bmatrix} 1 \\ 1 \\ 1 \end{bmatrix} e_l \end{aligned} \tag{5}$$

With $\boldsymbol{I} = [i_1 \ \ i_2 \ \ i_3]^t$ the state vector whose 3 components are the 3 ICT inner currents, $\boldsymbol{D} = [d_1 \ \ d_2 \ \ d_3]^t$ the control vector and e_l the scalar perturb input.

It is worth noting that the load voltage source represents a battery or the capacitive input filter of an inverter. This means that the series resistance r_l is low and can be neglected in a first approach. With this assumption, the

resulting state-space representation is:

$$\frac{d}{dt}\boldsymbol{I} = \mathrm{A}\boldsymbol{I} + B\boldsymbol{D} + B_p e_l \tag{6}$$

With A the state matrix and B the control matrix and B_p the perturb matrix described as:

$$A = \frac{-r}{(l-2m)\,(l+m)}\begin{bmatrix} l-m & m & m \\ m & l-m & m \\ m & m & l-m \end{bmatrix}$$

$$B = \frac{v_i}{(l-2m)\,(l+m)}\begin{bmatrix} l-m & m & m \\ m & l-m & m \\ m & m & l-m \end{bmatrix}$$

$$B_p = -\frac{1}{(l-2m)}\begin{bmatrix} 1 \\ 1 \\ 1 \end{bmatrix}$$

Note that the term r is voluntary not factored into the state equation to underline that the forthcoming robustness analysis of each control strategy considers individual winding resistance variation.

Functionally, the output current i_o, sum of the three winding currents (3), is the only variable which should be controlled. In actual experience, the converter faces discrepancies at several level (winding and switch resistances due to temperature difference, actual duty cycle of the switch due to non-identical dead-time, as examples) which may generate large DC current mismatch between each winding. It is hence mandatory to control each individual current i_k. In this context, the output vector is the state vector.

2.3. Model analysis

From an engineer point of view, it is important to describe the model behavior regarding the single common mode and the two differential modes, named com and $diff_1$, $diff_2$, respectively and defined by the following relations:

$$\begin{cases} x_{com} = (1/3)\,.\,(x_1 + x_2 + x_3) \\ x_{diff1} = x_1 - x_2 \\ x_{diff2} = x_2 - x_3 \end{cases} \tag{7}$$

Indeed, in normal operating mode, the supervisor splits the output current demand into three similar ICT's inner current. Hence, only the common mode is solicited while the two other differential modes remain zero. Conversely, while a default occurs like a local overheat affecting a specific cell, the supervisor decreases the related current and increases the two other ones creating no common change but two differential mode changes.

Substituting (7) in the state equation derives the open loop modes' behavior:

$$\begin{cases} \dfrac{d}{dt}i_{\mathrm{com}} = -\dfrac{1}{\tau_{com}}i_{\mathrm{com}} + \dfrac{v_i}{(l-2m)}d_{\mathrm{com}} - \dfrac{1}{(l-2m)}e_l \\ \dfrac{d}{dt}i_{\mathrm{diff1}} = -\dfrac{1}{\tau_{diff}}i_{\mathrm{diff1}} + \dfrac{v_i}{(l+m)}d_{\mathrm{diff1}} \\ \dfrac{d}{dt}i_{\mathrm{diff2}} = -\dfrac{1}{\tau_{diff}}i_{\mathrm{diff2}} + \dfrac{v_i}{(l+m)}d_{\mathrm{diff2}} \end{cases} \tag{8}$$

with τ_{com} and τ_{diff} the two different time constants of common mode and differential mode, respectively:

$$\tau_{com} = \frac{(l-2m)}{r}$$

$$\tau_{diff} = \frac{(l+m)}{r}$$

For the converter under study, the evaluation of the time constant values ratio is:

$$\frac{\tau_{com}}{\tau_{diff}} = \frac{l-2m}{l+m} = \frac{1}{29.5} \tag{9}$$

Table 2
Closed loop system specification.

Symbol	Quantity	Value
ε_i	Steady state offset	0
τ_{i_o}	Time-response (settling time)	500 (μs)
$\Delta\%_{i_k/i_k}$	Percentage overshoot regarding i_k subject to $i_{k,ref}$ setpoint change	10%
$\Delta\%_{i_j/i_k}$	Percentage overshoot regarding $i_{j\neq k}$ subject to $i_{k,ref}$ setpoint change	10%
DR	Maximum decay ratio	20%

It is hence clear that the open-loop system has two very different dynamics, which requires a specific control design. By nature, the circulating current can change slowly, while the output current can be adjusted very quickly, which is one of the main ICT's asset.

2.4. State feedback specifications

The control design has to take this detailed analysis into account with relevant required dynamics. The present study considers the specifications summarized in Table 2. Indeed, the first requirement is to guarantee a good precision in steady state in order to fulfill the maximum point tracker requirements; the purpose of the present study is to cancel the steady state error. Second, the time taken for the response to reach the desired set point is also important for the system functionality. The solar converter needs to react to solar irradiance changes which in the worst case may occur in a 10 ms time period, which is not very challenging. However, there are obviously other scenarios to consider; short circuit limitation is one of the cases requiring a rapid action. For this demanding challenge the settling time is set to 500 μs which means ten switching periods ($T_S = 50$ μs). A third key point is to ensure a good stability margin of the closed loop system. This point is achieved by satisfying an overshoot criteria and decay ratio. The overshoot criteria gives also a good indication on how duty cycles saturations are managed and is set to a maximum of 10%, while the decay ratio criteria gives a good performance index of the system stability and is limited to a maximum 20% value. In addition, the minimization of the windings currents coupling permits to control independently each phase current which is essential to modify the phase power distribution in case of a local overheating; the limited overshoot while another current is changing is a way to take this fact into account.

Finally, it is worth noting that the load voltage source represents a battery or the capacitive input filter of an inverter. Consequently, this voltage varies slowly and is measured for regulation purpose. Hence e_l represents a perturbation which can be simply cancelled by an additional feedforward term. More specifically, the control value $\boldsymbol{D}$ is the sum of two terms, one $\boldsymbol{D}_{e_l}$ computed using the output voltage measurement and the other one $\boldsymbol{D}'$ computed by the feedback law:

$$\boldsymbol{D} = \boldsymbol{D}_{e_l} + \boldsymbol{D}' = \begin{bmatrix} e_l/v_i \\ e_l/v_i \\ e_l/v_i \end{bmatrix} + \boldsymbol{D}' \tag{10}$$

In sum, that is the reason why the load voltage source will no longer be considered, as mentioned in Table 1.

3. State feedback

The previous section described the power converter behavior using a state representation [18,21]. It allowed to better understand the effects of the ICT magnetic coupling on the system. As it is easy to monitor each state variable using 3 current sensors, full state feedback seems to be a very appropriate control technique to adjust the characteristics of the closed loop system. A first step gives the overall control structure. Then the state feedback setting is considered showing a great number of possible tuning strategies. Among them, two specific methods showing particular promise are identified.

3.1. Control structure and the related extended model

The basic principle of state feedback [14,20] is to place the closed loop system poles using the following linear control law:

$$\boldsymbol{D} = -\boldsymbol{K}\boldsymbol{I} + \boldsymbol{F}\boldsymbol{I}_{ref} \tag{11}$$

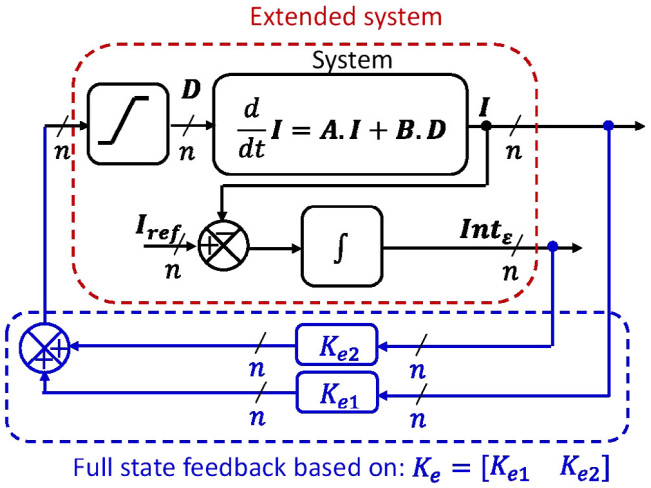

Fig. 2. Extended system with full state feedback.

where

- the $n \times n$ feedback matrix $\boldsymbol{K}$ enables to achieve the desired pole placement, which determines the system behavior.
- the $n \times n$ pre-filter matrix $\boldsymbol{F} = \boldsymbol{B}^{-1}(\boldsymbol{BK} - \boldsymbol{A})$ ensures a unit static gain between the reference values and the measured values. It is important to stress that this matrix is calculated with the state and control matrices ($\boldsymbol{A}$ and $\boldsymbol{B}$) and thus strongly depends on the system parameters.

Obviously, due to the mandatory pre-filter matrix, this first control structure is strongly dependent on system parameters uncertainties. The way to deal with this is to add integral terms to the feedback structure. It provides a suitable solution enabling to strengthen the overall feedback robustness and guarantee no static error in any case. The idea is first to integer the errors between the references and the related currents and then consider the three integer outputs as three additional system states. Consequently the extended state dimension is $n_e = 2n = 6$ and its state representation is described by:

$$\frac{d}{dt}\begin{bmatrix} \boldsymbol{I} \\ \boldsymbol{Int_\varepsilon} \end{bmatrix} = \begin{bmatrix} \boldsymbol{A} & \boldsymbol{0_3} \\ -\boldsymbol{Id_3} & \boldsymbol{0_3} \end{bmatrix}\begin{bmatrix} \boldsymbol{I} \\ \boldsymbol{Int_\varepsilon} \end{bmatrix} + \begin{bmatrix} \boldsymbol{B} \\ \boldsymbol{0_3} \end{bmatrix}\boldsymbol{D} + \begin{bmatrix} \boldsymbol{0_3} \\ \boldsymbol{Id_3} \end{bmatrix}\begin{bmatrix} \boldsymbol{I_{ref}} \end{bmatrix} \tag{12}$$

3.2. Control structure degrees of freedom

Similarly to the basic state feedback, the control values $\boldsymbol{D}$ are calculated using the full state knowledge as depicted in Fig. 2. Note that the reference values $\boldsymbol{I_{ref}}$ no longer act directly on the control values but through an integral path which filters the set point variations. Consequently, it avoids temporal overshoots of output values during fast transient.

To compute the 3 control values (i.e. $\boldsymbol{D}$), the state feedback linearly combines 6 states (i.e. $[\boldsymbol{I}\,\boldsymbol{Int_\varepsilon}]^t$). The following equation gives the related full feedback control law:

$$\boldsymbol{D} = -\boldsymbol{K_e}\begin{bmatrix} \boldsymbol{I} \\ \boldsymbol{Int_\varepsilon} \end{bmatrix} \tag{13}$$

The $n \times n_e$ feedback matrix $K_e = [K_{e1}\ K_{e2}]$ has $n \times n_e = 18$ independent real parameters. For greater readability, the $\boldsymbol{K_e}$ matrix is split into two submatrices. K_{e1} represents a $n \times n$ matrix made of the n first K_e columns: it contains the $\boldsymbol{I}$ weighting parameters. Likewise, K_{e2} is a similar matrix consisting of the n last K_e columns and has the $\boldsymbol{Int_\varepsilon}$ weighting parameters.

Adjusting the $\boldsymbol{K_e}$ eighteen parameters permits to choose the $n_e = 6$ poles of the closed loop system which has a strong influence on the system's dynamics. It is thus evident that the $\boldsymbol{K_e}$ matrix meeting this pole criteria is

not unique. To take advantage of the opportunities offered by these too many coefficients, it is important to make explicit additional criteria permitting to strictly define them.

- One solution that could be explored would be obtaining a total $\boldsymbol{K_e}$ decoupling for the 6 states. This additional constraint gives a unique solution.
- Another option is to compute the feedback matrix which minimizes a quadratic index performance based on a combination of states and control values.

Both possibilities are evaluated in the next sections regarding

- The performances in rated conditions,
- The robustness towards parameter uncertainties,
- The ease of implementation.

4. Decoupling strategy

This section focuses on the first identified option which consists in dynamically decoupling [15,16] the link between current references and current responses. Its specific tuning is explained and then computed.

4.1. Specific tuning leading to a decoupled feedback

Combining the extended state equation (12) and the full feedback control law (13) derives the close loop behavior described by:

$$\frac{d}{dt}\begin{bmatrix} \boldsymbol{I} \\ \boldsymbol{Int_\varepsilon} \end{bmatrix} = \boldsymbol{A_{e,CL}}\begin{bmatrix} \boldsymbol{I} \\ \boldsymbol{Int_\varepsilon} \end{bmatrix} + \boldsymbol{B_{e,CL}}\begin{bmatrix} \boldsymbol{I_{ref}} \end{bmatrix} \tag{14}$$

where $\boldsymbol{A_{e,CL}}$ represents the $n_e \times n_e$ closed loop state matrix and $\boldsymbol{B_{e,CL}}$ is the $n_e \times n$ closed loop control matrix. The latter are defined as follows:

$$\boldsymbol{A_{e,CL}} = \begin{bmatrix} \boldsymbol{A} - \boldsymbol{B}.\boldsymbol{K_{e1}} & -\boldsymbol{B}.\boldsymbol{K_{e2}} \\ -\boldsymbol{Id_3} & \boldsymbol{0_3} \end{bmatrix}$$

$$\boldsymbol{B_{e,CL}} = \begin{bmatrix} \boldsymbol{0_3} \\ \boldsymbol{Id_3} \end{bmatrix}$$

The characteristics of the system response is fully determined by the value of the $n \times n_e = 18$ adjustable terms of the closed-loop state matrix, namely the first n rows of this matrix. It is sought to impose:

- First the $n_e = 6$ eigenvalues in order to settle the overall closed loop dynamics. Writing the characteristic equation and identifying it with its desire form leads to $n_e = 6$ non-linear equations.
- Second a cancellation of the coupling effect between the three windings currents. For instance, i_2 and i_3, as well as $int_{\varepsilon 2}$ and $int_{\varepsilon 3}$, must no longer impact the time-derivative of the first current di_1/dt. In sum, the closed loop matrix must also conform to the following form:

$$A_{e,CL} = \begin{bmatrix} a_{11} & 0 & 0 & a_{14} & 0 & 0 \\ 0 & a_{22} & 0 & 0 & a_{25} & 0 \\ 0 & 0 & a_{33} & 0 & 0 & a_{36} \\ -1 & 0 & 0 & 0 & 0 & 0 \\ 0 & -1 & 0 & 0 & 0 & 0 \\ 0 & 0 & -1 & 0 & 0 & 0 \end{bmatrix} \tag{15}$$

  Finally, $(n \times n_e) - n_e = 12$ independent linear equations can be deduced from this imposed matrix structure.

In conclusion, this first strategy leads to solve a system of $n \times n_e = 18$ equations with $n \times n_e = 18$ unknowns.

Table 3
Coefficients of the decoupling full state feedback.

K_{e1}			K_{e2}		
2.033	−1.933	−0.967	−12 000	11 600	5800
−0.967	1.067	−0.967	5800	−6400	5800
0.000	0.000	3.000	0	0	−1800

4.2. Matrix gain related to decoupling strategy

It can be achieved using a specific solver based on formal calculation or numeric computation. The latter technique that was used here. The final results are shown in Table 3. Most of the coefficients of the feedback gain matrix K_e are nonzero. None of the square sub-matrices (namely K_{e1} and K_{e2}) are diagonal which reveals a very coupled feedback. All state variables are really necessary to compute one of the 3 control values d_k.

This finding impacts significantly both the controller implementation and the global system behavior. Indeed, during large fluctuation of the set point, the control law will temporarily compute large control values. In practice, the duty cycle will be saturated to its own limits. Saturation causes an open-loop behavior, which is especially detrimental to integral terms that continue to evolve. Integral terms then lead to large unexpected overshoot and possibly instability while saturation occurs. Anti-windup systems [4,10,19] intend to maintain the system in close loop. However, saturation is a non-linear phenomenon. In the present case of non-diagonal submatrices, it is not possible to know with certainty which of the integral terms induce saturation. Hence in any saturation situation the anti-windup system clamps the three integral actions. This conservative option leads to a sub-optimal implementation of the controller.

In sum, the strict decoupling option has two theoretical drawbacks. It leads to a large number of multiplications and it results in an inadequate anti-windup implementation.

Next section presents the second approach, in order to be able to compare them using simulation MATLAB tool.

5. Linear quadratic regulator (LQR)

5.1. Objective function

An alternate way to address the setting parameters design issue of the full state feedback is to settle the degrees of freedom and flexibility using a global performance index summarizing the closed loop behavior. It involves a functional, namely a time infinite-horizon Riemann integral based on a quadratic cost function:

$$J = \int_0^{\infty} \left(\begin{bmatrix} I \\ Int_{\varepsilon} \end{bmatrix}^t .Q. \begin{bmatrix} I \\ Int_{\varepsilon} \end{bmatrix} + D^t.R.D \right) .dt \tag{16}$$

where Q and R are two positive semi-definite matrices of weighting factors for the various state and control components, respectively. As in this case, any current i_k plays the same role and similarly any duty cycle d_k applies the same way, Q and R are simplified to $Q = \begin{bmatrix} Id_3 & 0_3 \\ 0_3 & q.Id_3 \end{bmatrix}$ and $R = \rho.Id_3$.

In conclusion, the objective is to find the (q, ρ) set of two scalar values that best meets specification (given in Table 2). For this purpose, each (q, ρ) set permits to compute a full state feedback $D = -K_e.[I \;\; Int_{\varepsilon}]^t$ that minimizes the cost function:

$$J(q, \rho) = \int_0^{\infty} \left(\begin{bmatrix} I \\ Int_{\varepsilon} \end{bmatrix}^t . \begin{bmatrix} Id_3 & 0_3 \\ 0_3 & q.Id_3 \end{bmatrix} . \begin{bmatrix} I \\ Int_{\varepsilon} \end{bmatrix} + D^t.\rho.Id_3.D \right) .dt \tag{17}$$

To determine the first optimization level, namely the full state feedback settings, Riccati equation is used. The choice of the 2 weighting coefficients is the second step which is realized using a genetic algorithm [5]. It permits to settle the actual degree of freedom of LQR approach.

Table 4
LQR design of the full state feedback strategy setting parameters.

K_{e1}			K_{e2}		
0.564	−0.154	−0.154	−3162	0	0
−0.154	0.564	−0.154	0	−3162	0
−0.154	−0.154	0.564	0	0	−3162

5.2. Matrix gain related to LQR strategy

Based on this LQR design approach [5,12], the global full state feedback is designed. It leads to the parameters listed in Table 4. It actually seems that most the K_{e2} gain matrix related to the integral terms is strictly diagonal and that the K_{e1} gain matrix related to the proportional terms has dominant values in the diagonal line. In concrete terms this means the controller acts as if it was three independent controllers acting independently on their dedicated duty cycle. In this context, it leads to a fewer number of multiplication, but above all to a simple and efficient anti-windup scheme because the reason for a saturation effect can be easily attributed to the related integral term.

6. Comparative simulations results

To illustrate the dynamic properties of both feedback design approaches, this section shows the closed loop system response while it is subject to three specific current reference changes, namely stimulation of the common mode, of the differential modes and finally of both modes. The initial condition is set so that the converter provides 6 A to the load (200 V voltage source) equitably shared by the three ICT windings (2 A). This equilibrium point corresponds to 3 duty cycles close to 50%.

In this first step, the system is considered with the same rated parameters as those used to tune the controller.

6.1. Common mode response

For this trial, all current references have a similar 500 Hz square generator with 2 A as low level and 4 A as high level. Fig. 3 reports the corresponding results of both strategies.

As planned by the decoupling theory, the winding currents evolve simultaneously while satisfying the 500 µs time settling requirement, as shown in Fig. 3(a). The common-mode and differential-mode currents confirm this assessment by showing no response on the two differential mode channels. To get this effect, the controller only slightly changes the duty cycle amplitude which is consistent with the small common mode open-loop time constant.

Fig. 3(b) shows the LQR results. It also complies with the 500 µs time settling requirement, having faster time response than the previous one. As an illustration of this phenomenon, it can be noticed that the control overshoot values are roughly 60% higher than in the decoupling case. Nevertheless, as in this last case, the control value fluctuations remain low.

6.2. Differential mode response

Fig. 4 shows the results of the situation where the first current reference $i_{1,ref}$ has a 2/3 A ripple magnitude while the two others are set in opposite phase with half the magnitude, namely 1/3 A.

Regarding the decoupling approach depicted in Fig. 4(a), each current has the same dynamics as the common mode one. On the other hand, the different duty cycles have a large transient overshoot which is explained by the need to compensate the slow natural differential mode dynamics. Indeed the natural response time value is thirty times higher than the common mode one. Anyway, as expected by the theoretical part, the fictitious currents show a unique mode evolution (first differential mode) while the two other channels (i.e. common mode and second differential mode) have no reaction. The closed loop decoupling is therefore entirely satisfied.

The LQR approach shows different results. As demanded by the specification, the differential mode satisfies the 500 µs time settling requirement, but it has a slower dynamics than the common mode one. Contrary to the previous strategy, the LQR method derives a control that makes both modes dynamics different. This result is not surprising given that LQR has a global approach combining both error and control magnitudes issues. As differential mode is

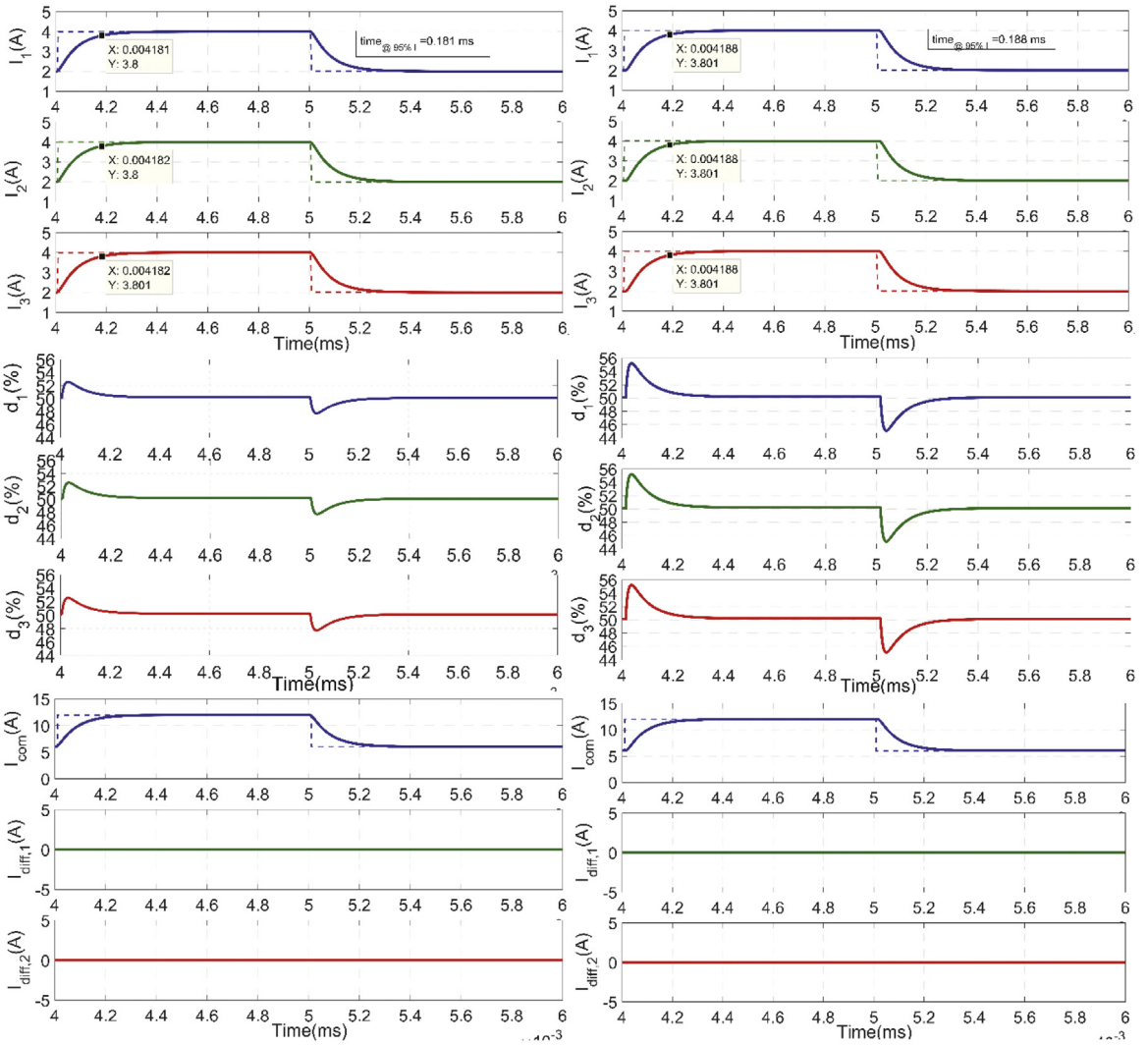

Fig. 3. Closed loop common mode response.

slow, it provides the minimum required gain values. As already noted, these gain values make the common mode faster due to its intrinsic high dynamics. It can be noticed in Fig. 4 that the control overshoot values are roughly 15% lower than in the decoupling case. This tuning difference would have an impact on the single step response illustrating the case of a desired channel mismatch due to cell discrepancies, such as cell overheating. This further trial activates simultaneously both common and differential modes.

6.3. Single mode response

Finally, Figs. 5 and 6 depict the results corresponding to the configuration where the supervision strategy needs to use unbalanced windings currents, for instance to take the pressure off a warmer cell. To make this last point, only the first current reference $i_{1,ref}$ changes with a step magnitude of 2 A (see Fig. 5) and then 3 A (see Fig. 6). This trial solicits both the common mode and the first differential mode.

As far as the decoupling strategy is concerned, the first trial shows input–output decoupling resulting from the fact that each natural mode behaves with similar time response. As this situation solicits two out of the three system

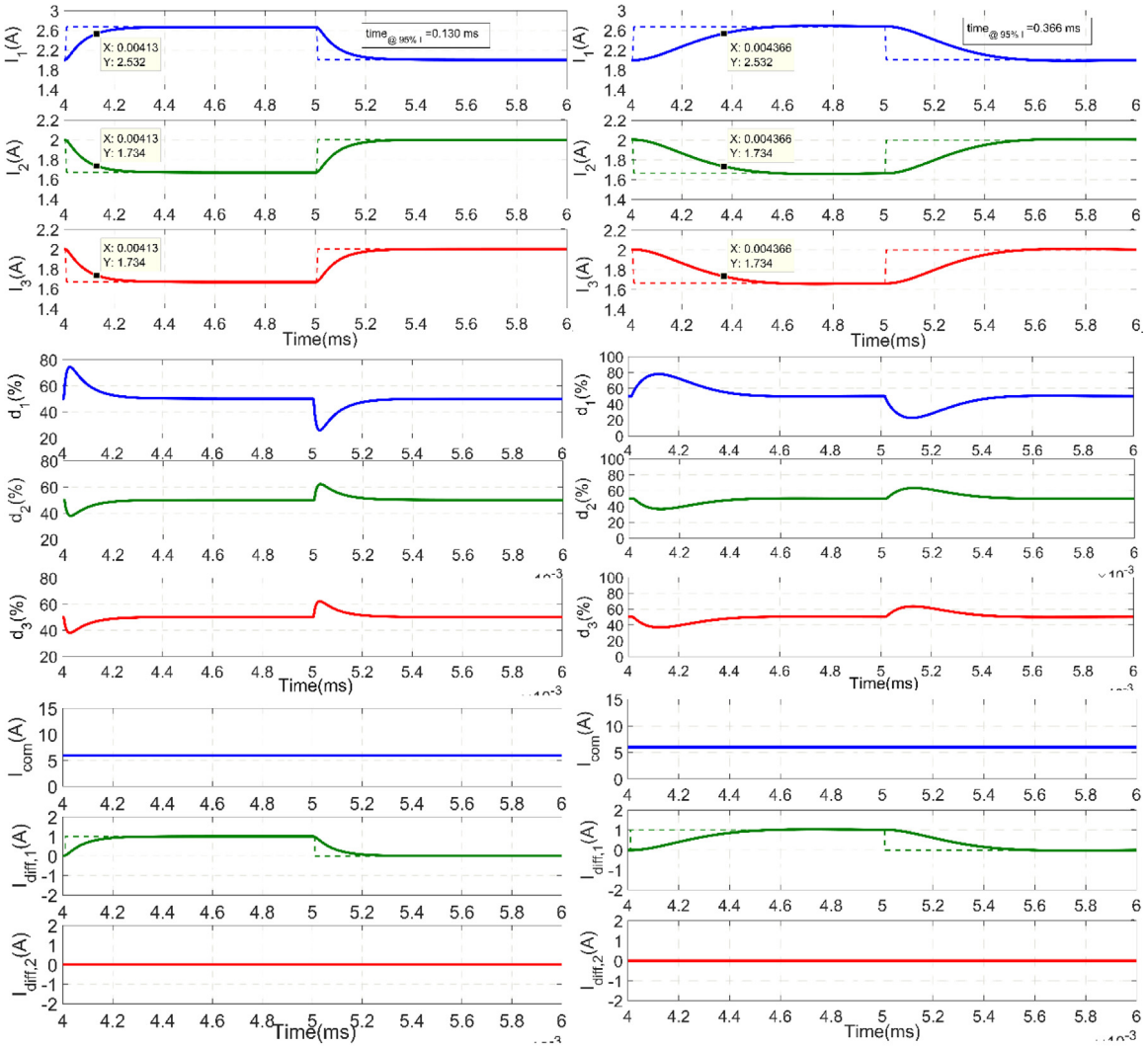

a) Decoupling approach b) LQR approach

Fig. 4. Closed loop differential mode response.

modes, it is also not surprising to note that duty cycles react strongly. However Fig. 6 shows a coupling effect. That has been tied to the fact that one duty cycle tends transiently to exceed its limit value: the anti-windup apparatus operates and introduces a non-linearity which cancels the decoupling effect. This phenomenon disappears as soon as anti-windup function is useless.

Fig. 5(b) depicts the first current step response behavior of the LQR method. Compared to Fig. 5(a), the LQR design induces a much less aggressive control law which maintains the duty cycles much easily within its limits. Conversely, the first current change impacts slightly the two others without exceeding the specifications. It arises because the common mode and differential mode dynamics are different this time.

Fig. 6(b) also illustrates that the present controller may be almost considered as composed of three independent controllers. Indeed, Fig. 6(b) shows in dashed lines the same transient response in the case where all non-diagonal terms of K_{e1} are set to zero. Even if the coupling effects is somewhat increased, the behavior remains similar and totally acceptable. That is the reason why the anti-windup apparatus can be properly built by impacting solely the integral term corresponding to the control variable in saturation. Moreover it leads to a very simple implementation similar to SISO systems. Fig. 6-b depicts the very good functioning of this implementation. It should be specified

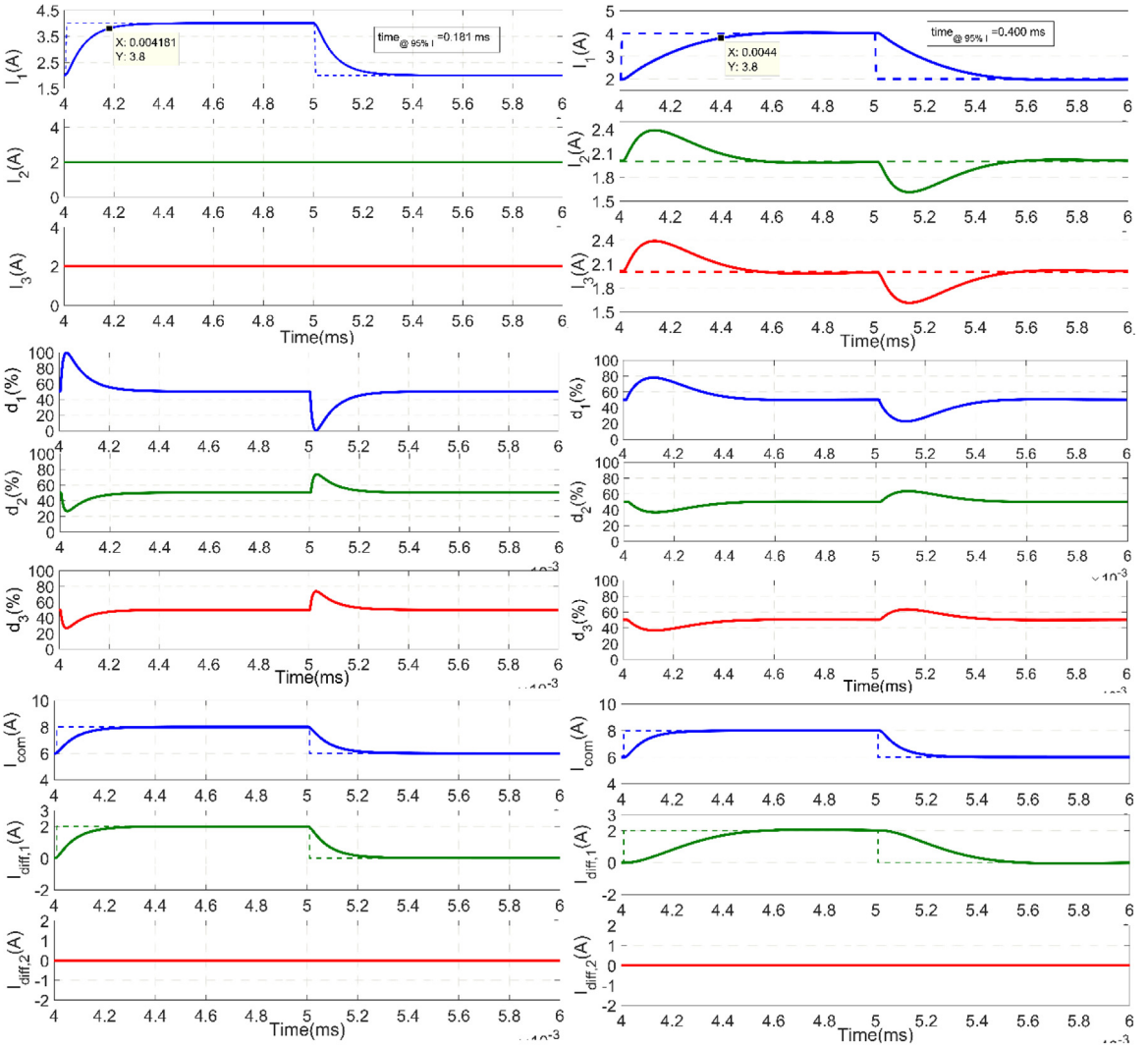

a) Decoupling approach b) LQR approach

Fig. 5. Closed loop single step response : small signal.

that the step magnitude has to be enlarged in Fig. 6(b) compared to Fig. 6(a), in order to reach saturation mode. It is clearly due to the less aggressive behavior of the LQR approach compared to the decoupling one. For information, in the present case, only the first duty cycle is saturated and consequently the first integer is stopped simply if the first duty cycle is clamped to 100% and the current error is positive, or the first duty cycle is clamped to 0% and the current error is negative.

6.4. Sensitivity analysis

This second step investigates the sensitivity of both designs towards ICT parameters. Self-inductance and mutual inductance are studied as critical parameters to assess the control robustness.

Considering decoupling design, a better ICT coupling cancels the perfect coupling rejection as depicted in Fig. 7-a where the actual values are $l = 19.8$ mH and $m = 9.7$ mH. It induces a shift of the natural common mode dynamics (smaller time response) which finally also induces a close loop common mode settling time. This change is mitigated

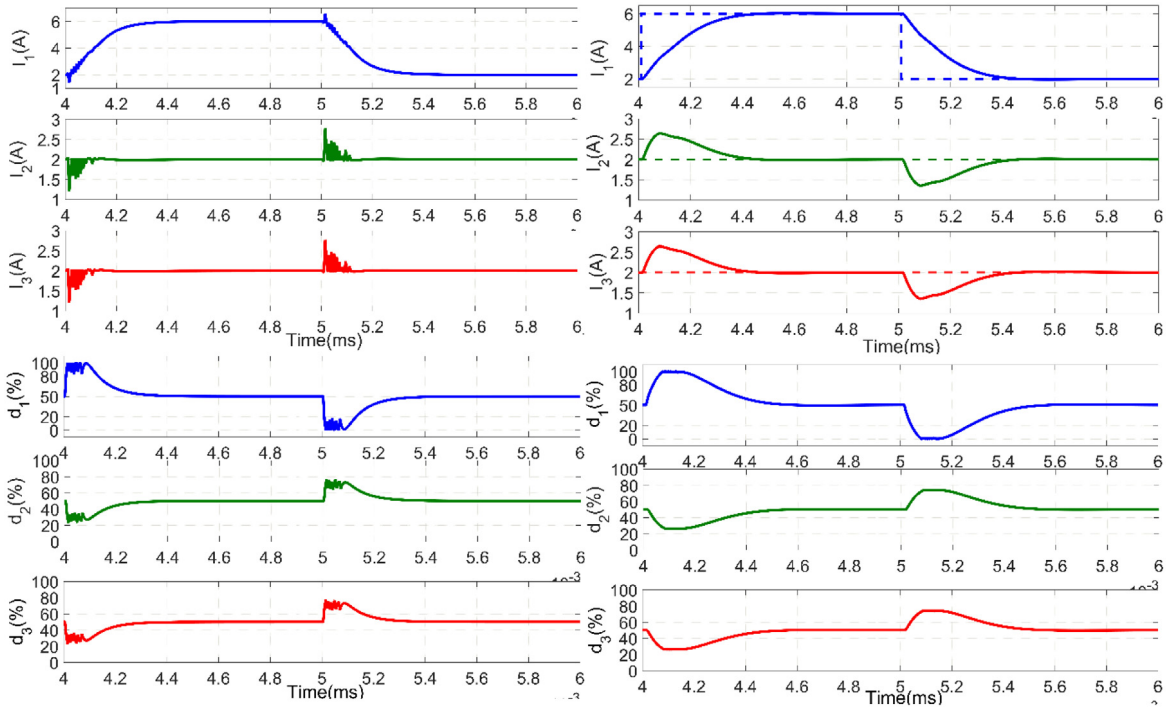

a) Decoupling approach b) LQR approach

Fig. 6. Closed loop single step response : large signal.

by the controller but it induces a mismatch between the different modes dynamics which in turn produces this temporal channel coupling effect. In the case of an even better ICT coupling, the close loop behavior can also face instability as reported in Fig. 8-a, where $l = 19.7$ mH and $= 9.8$ mH .

Besides a smoother control action and a simpler implementation in a controller, the LQR design proves a better robustness regarding parameters uncertainty. As a matter of fact, Figs. 7-b and 8-b show that the controller remains stable even in the most demanding case of a higher actual ICT coupling than expected, namely when l = 19.7 mH and m = 9.8 mH.

6.5. Overview of the simulation results

In summary, it can be said that the decoupling strategy leads to a controller easy to implement with a modal approach. However, it reveals limited in the case of a good ICT coupling because it requires high gains to boost low natural dynamics, namely differential mode, and becomes hence sensitive to noise injection and sampling effects. In addition, the real implementation does not exhibit a very efficient anti-windup scheme. Last but not least, the closed loop behavior is somewhat sensitive to parameters which is not appropriate for a robust control. That is why linear quadratic regulator [5,12] design is much better to considered. It respects the various specifications demand, provides smooth control in the present case of a large range of natural dynamics and ensures a very robust response towards parameters change.

7. Conclusion and perspectives

The present study addresses the easier and more robust way to implement a controller scheme dedicated to control the current in an interleaved multi-cell converter using an ICT. The study is based on a specific 3-cell converter, but it draws generalizable conclusions about control of interleaved converters, whatever the number of cells. ICT device clearly enables to significantly reduce both input and output currents ripples which permits using reliable

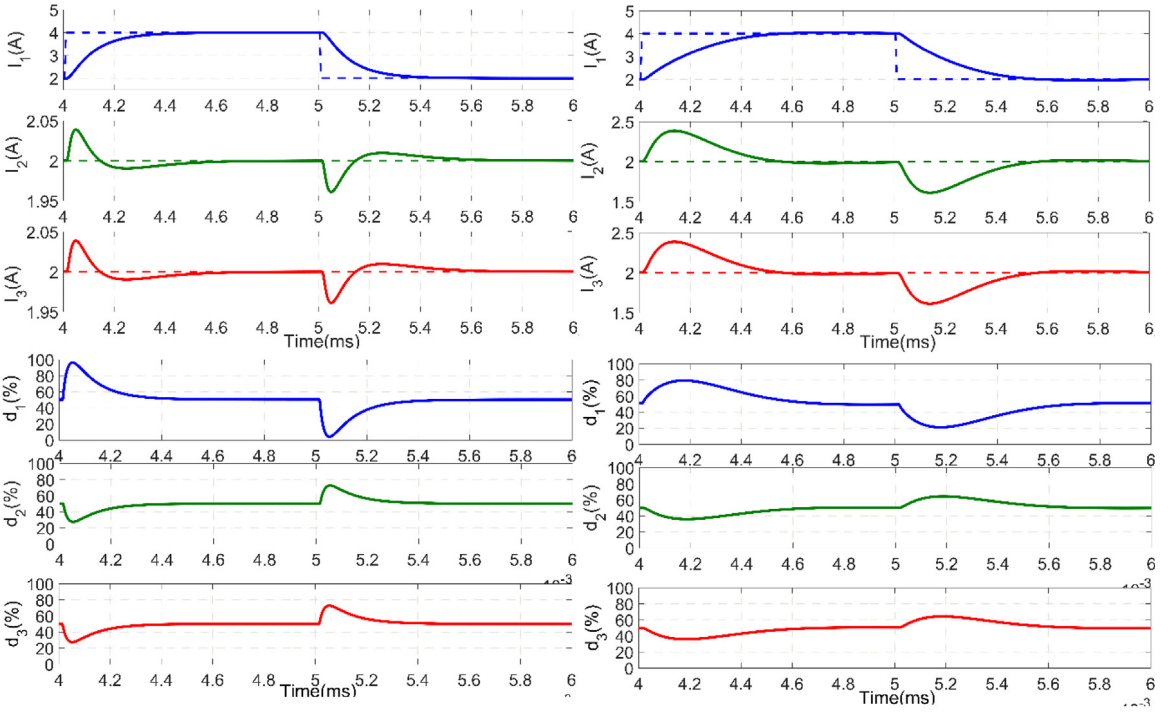

a) Decoupling approach b) LQR approach

Fig. 7. Closed loop single step response with small ICT parameters change. (L = 19,8 mH and M = 9,7 mH).

capacitor technology. However, the ICT magnetic coupling induces to deal with a real MIMO system. To cope with this issue, two different approaches are assessed.

The first one based on a modal method is easy to understand for an engineering point of view. While operating in linear mode and with rated values, it permits a very good decoupling between the references inputs and the related outputs. However, an efficient anti-windup scheme cannot be implemented to optimally take the duty cycles saturation into account. Moreover, the control design reveals somewhat sensitive to the ICT parameters which may be difficult to evaluate precisely. Finally, it uses high gains to offset the slow natural dynamics of the differential mode, possibly leading to noise sensitivity and more frequent saturated behavior.

The second methodology is based on a full state feedback of an extended model whose parameters are set using a quadratic cost time function. This so-called LQR technique enables to find a good trade-off between the different key points of the specification, which are stability, settling time, decoupling and robustness. Although a small but acceptable coupling remains, this second controller exhibits an almost internally decoupled structure permitting to implement a simple and efficient anti-windup technique. In addition, the controller acts smoothly during transient which reduces noise sensitivity. Finally it reveals more robust to ICT parameters changes, which is an important asset.

All these studies carried out in simulation show that the interleaved multi-cell converter is a very specific power converter. In this particular case, the full state feedback approach based on LQR method exhibits a very attractive trade-off between the different requirements of the control specifications while enabling a very easy implementation in a microcontroller or a FPGA device. These very positive results encourage to validate the study with an experiment on a laboratory test bench.

From a broader perspective, the present work shows to the power electronics community that there is a genuine benefit in switching from decoupling approach to LQR methodology. Whatever the system under study, decoupling strategy is proving to be much more sensitive to parameter changes and provides larger control values in case of a

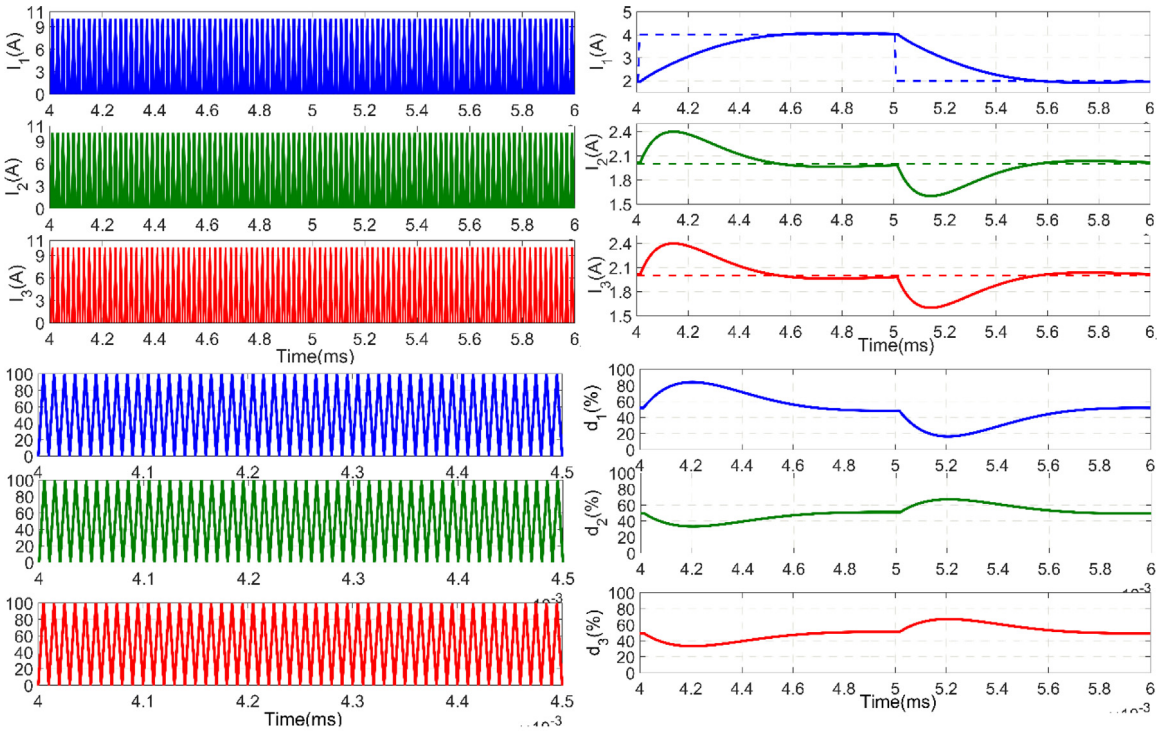

a) Decoupling approach b) LQR approach

Fig. 8. Closed loop single step response with small ICT parameters change. (L = 19,7 mH and M = 9,8 mH).

significant difference between natural dynamics. Conversely, if some small cross-coupling may be permitted, LQR tuning provides a robust and smooth control, which is extremely satisfying from an engineering point of view.

References

[1] B. Amghar, M. Darcherif, J.-P. Barbot, P. Gauthier, Modeling and control of parallel multicell choer using Petri nets, in: IFAC Proceedings Volumes, Vol. 45, 2012, pp. 633–638.

[2] M.L. Bolloch, M. Cousineau, T. Meynard, Current-sharing control technique for interleaving VRMs using intercell transformers, in: 2009 13th European Conference on Power Electronics and Alications, 2009, pp. 1–10.

[3] Y. Cho, Dual-buck residential photovoltaic inverter with a high-accuracy repetitive current controller, Renew. Energy 101 (2017) 168–181.

[4] Frederik M. De Belie, Peter Sergeant, Jan A. Melkebeek, A sensorless PMSM drive using modified high-frequency test pulse sequences for the purpose of a discrete-time current controller with fixed sampling frequency, Math. Comput. Simulation 81 (2) (2010) 367–381.

[5] F.H. Dupont, V.F. Montagner, J.R. Pinheiro, H. Pinheiro, S.V.G. Oliveira, A. Péres, Comparison of linear quadratic controllers with stability analysis for DC-DC boost converters under large load range, Asian J. Control 15 (3) (2013) 861–871.

[6] M. Elsied, A. Oukaour, H. Chaoui, H. Gualous, R. Hassan, A. Amin, Real-time implementation of four-phase interleaved DC–DC boost converter for electric vehicle power system, Electr. Power Syst. Res. 141 (2016) 210–220.

[7] C. Gautier, F. Adam, E. Laboure, B. Revol, D. Labrousse, Control for the currents balancing of a multicell interleaved converter with ICT, in: 2013 15th European Conference on Power Electronics and Alications (EPE), 2013, pp. 1–9.

[8] D. Guilbert, A. Gaillard, A. N'Diaye, A. Djerdir, Power switch failures tolerance and remedial strategies of a 4-leg floating interleaved DC/DC boost converter for photovoltaic/fuel cell alications, Renew. Energy 90 (2016) 14–27.

[9] D. Guilbert, A. N'Diaye, A. Gaillard, A. Djerdir, Fuel cell systems reliability and availability enhancement by developing a fast and efficient power switch open-circuit fault detection algorithm in interleaved dc/dc boost converter topologies, Int. J. Hydrogen Energy 41 (2016) 15505–15517.

[10] C.L. Hoo, Sallehuddin Mohamed Haris, Edwin C.Y. Chung, Nik Abdullah Nik Mohamed, New integral antiwindup scheme for PI motor speed control, Asian J. Control 17 (6) (2015) 2115–2132.

[11] E. Laboure, A. Cuniere, T.A. Meynard, F. Forest, E. Sarraute, A theoretical aroach to intercell transformers, alication to interleaved converters, IEEE Trans. Power Electron. 23 (1) (2008) 464–474.
[12] Wah Soon Lee, Machavaram Venkata Calapathy Rao, Modeling and design of tape transport mechanism, Math. Comput. Simulation 72 (1) (2006) 26–37.
[13] Yu. Li, Masato Ishikawa, Statistical analysis of power system sensitivity under random penetration of photovoltaic generation, Asian J. Control 19 (5) (2017) 1–11.
[14] E. Ostertag, Mono- And Multivariable Control and Estimation, Vol. 5, Springer, 2011, ISBN-10:3642137334.
[15] T.G. Pimenides, S.G. Tzafestas, Feedback decoupling-controller design of 3-D systems in state space, Math. Comput. Simulation 24 (4) (1982) 341–352.
[16] J. Ruiz-Leon, A.J. Sapiens, S. Čelikovsky, J.A. Torres, Decoupling with stability: alication to the real time control of a water storing plant, Asian J. Control 6 (3) (2004) 415–420.
[17] S. Sanchez, F. Richardeau, D. Risaletto, Design and fault-operation analysis of a modular cyclic cascade inter-cell transformer (ICT) for parallel multicell converters, Math. Comput. Simulation 131 (2017) 190–199.
[18] M. Shahin, S. Maka, State variable aroach to the analysis of neural control of long term blood pressure dynamics, Asian J. Control 13 (1) (2011) 164–176.
[19] K. Suyama, N. Sebe, Controller reset strategy for anti-windup based on switching L2 gain analysis, Asian J. Control 20 (1) (2018) 1–14.
[20] W.M. Wonham, On pole assignment in multi-input controllable linear systems, IEEE Trans. Automat. Control 12 (1967) 660–665.
[21] N. Yassa, M. Rachek, Modeling and detecting the stator winding inter turn fault of permanent magnet synchronous motors using stator current signature analysis, Math. Comput. Simulation 167 (2020) 325–339.
[22] N. Zhang, D. Sutanto, K.M. Muttaqi, A review of topologies of three-port DC–DC converters for the integration of renewable energy and energy storage system, Renew. Sustain. Energy Rev. 56 (2016) 388–401.